Basin-wide magnetostratigraphic framework for the Bighorn Basin, Wyoming

William C. Clyde†
Walid Hamzi
Department of Earth Sciences, University of New Hampshire, Durham, New Hampshire 03824, USA

John A. Finarelli
Committee on Evolutionary Biology, University of Chicago, Chicago, Illinois 60637, USA

Scott L. Wing
Department of Paleobiology, Smithsonian Institution, Washington, D.C. 20560, USA

David Schankler
68 Fieldcrest Avenue, Skillman, New Jersey 08558, USA

Amy Chew
Department of Anatomical Sciences, Stony Brook University, State University of New York, Stony Brook, New York 11794, USA

ABSTRACT

New paleomagnetic data from six different sections in the Bighorn Basin are combined with previously published results to construct a basin-wide magnetostratigraphic framework. Geomagnetic polarity reversals between chrons C26r, C26n, C25r, C25n, C24r, and C24n have been identified among multiple stratigraphic sections in different parts of the basin. Using the new magnetostratigraphic framework, paleontological, paleobotanical, and isotopic information from these varied locations in the basin can now be correlated and compared to similar records from elsewhere in the world. These new data resolve previous uncertainty concerning the timing of an important episode of faunal turnover known as Biohorizon B, which is slightly below the chron C24r-C24n boundary, close to the position of the Elmo isotope excursion in marine records. Backstripping analysis using these new magnetostratigraphic data helps define the time-transgressive onset of basin formation and shows the different subsidence histories of the northern and southern parts of the basin.

Keywords: magnetostratigraphy, Paleocene, Eocene, Bighorn Basin, mammals, plants.

INTRODUCTION

The Bighorn Basin of Wyoming preserves a remarkably continuous continental record of late Paleocene to early Eocene biotic and climatic change, but incomplete paleomagnetic data, asymmetric sediment accumulation rates, and differing biostratigraphic zonations have complicated efforts to make precise chronostratigraphic correlations among distant parts of the basin. Geomagnetic polarity reversals are ideal for making chronostratigraphic correlations because they are independent of lithostratigraphic variations and more precise than biostratigraphic correlations. Here we present new paleomagnetic data from six stratigraphic sections and combine them with previously published results to construct the first basin-wide magnetostratigraphic framework for the Bighorn Basin. This new framework helps tie together much of the paleontological and isotopic data from the basin into a single stratigraphic context and provides temporal limits on the initiation of basin formation and along-strike variability in subsidence.

Initial paleomagnetic research in the Bighorn Basin was carried out by Butler et al. (1981, 1987) in the northern part of the basin along Polecat Bench and in Big Sand Coulee (Fig. 1). That study recovered a continuous record from chron C27n to chron C24r and successfully tied many important Paleocene and early Eocene fossil localities from this area to the geomagnetic polarity time scale (GPTS). In an effort to extend the magnetostratigraphic record into younger deposits that do not crop out in the northern basin, Clyde et al. (1994, 2001) and Tauxe et al. (1994) sampled sections farther to the south and east. Clyde et al. (1994) reported paleomagnetic results from a 1480 m section in the McCullough Peaks area that extended from the Paleocene-Eocene (P-E) boundary to the Wa-7 faunal zone (Lostcabinian subage of the Wasatchian North American Land Mammal Age). Tauxe et al. (1994) reported results from the 750 m composite section of Bown et al. (1994) in the southern part of the basin that also spans from the P-E boundary into Wa-7, but extends even higher into the overlying Tatman Formation. Secord et al. (2006) reported paleomagnetic results from three sections (Princeton Quarry, Cedar Point Quarry, and Croc Tooth Quarry sections) in the Foster Gulch area of the northern Bighorn Basin, extending the magnetostratigraphic framework for that area into the lower part of the Fort Union Formation. The addition of six new magnetostratigraphic sections presented here provides a much more spatially complete chronostratigraphic framework for the basin and helps resolve apparent discrepancies between biostratigraphic events and the pattern of magnetic polarity reversals.

METHODS

We collected 3 or more oriented paleomagnetic samples from 169 sites in 6 different stratigraphic sections throughout the basin. Strati-

†will.clyde@unh.edu

GSA Bulletin; July/August 2007; v. 119; no. 7/8; p. 848–859; doi: 10.1130/B26104.1; 10 figures; 1 table; Data Repository item 2007145.

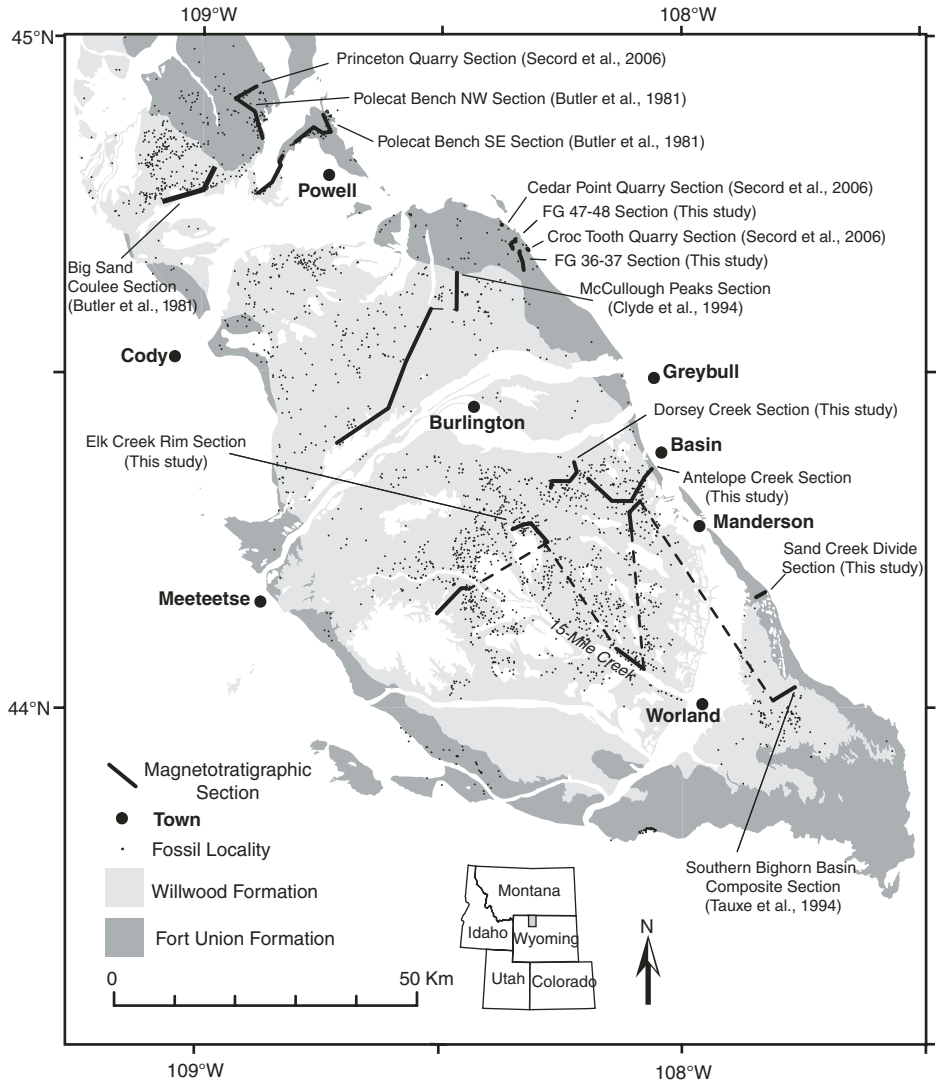

Figure 1. Geologic map of Bighorn Basin showing locations of previously and newly sampled magnetostratigraphic sections (dark lines) and spatial distribution of fossil localities (small points).

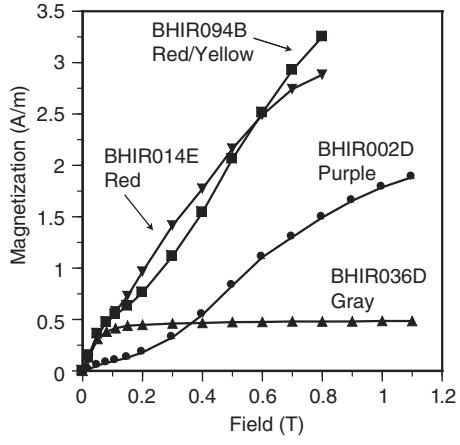

Figure 2. Acquisition curves of isothermal remanent magnetization (IRM) along the *Z* axis up to a maximum of 1.1 T for samples from different facies in the Bighorn Basin. The purple (BH01002D), red (BH01014E), and red and yellow (BH01094B) samples are all from the Willwood Formation and show smooth acquisition of IRM without reaching saturation, indicating the presence of a high-coercivity mineral like hematite or goethite. The gray sample (BH01036D) is from the Fort Union Formation and shows smooth acquisition of IRM up to 0.15 T before reaching saturation, indicating the presence of a low-coercivity mineral like magnetite.

graphic sections were measured using Jacob staff and abney level. Global positioning system location and stratigraphic level were determined for each sample site. Facies targets and demagnetization protocols for different formations were determined by analysis of pilot samples and by evaluating previously published results (Butler et al., 1981; Clyde et al., 1994; Tauxe et al., 1994). Samples from the Willwood Formation were predominantly collected from paleosol mudstone deposits and were stepwise thermally demagnetized up to 690 °C. Samples from the Fort Union Formation were predominantly collected from unoxidized mudstones and were alternating field (AF) demagnetized up to peak fields of 100 mT. Magnetic mineralogy was further investigated for a suite of pilot samples representing different lithologies by the acquisition of isothermal remanent magnetization (IRM) up to a peak field of 1.1 T, and from thermal demagnetization of three mutually orthogonal IRMs of different intensities (Lowrie, 1990). In the latter experiment, the applied fields were 1.1 T along the *Z* axis, 0.4 T along the *Y* axis, and 0.12 T along the *X* axis. All analyses were conducted in the paleomagnetics laboratory at University of New Hampshire using an HSM2 SQUID cryogenic magnetometer, Molspin tumbling AF demagnetizer, an ASC Model TD48-SC thermal demagnetizer, and an ASC IM10 impulse magnet.

PALEOMAGNETIC RESULTS

IRM experiments suggest that the mudstones in the Willwood Formation and Fort Union Formation are quite different in terms of their magnetic mineralogy. We evaluated the IRM of three Willwood samples of differing color (red—BHIR014E, purple—BHIR002D, red with yellow mottles—BHIR094B) to determine if these color differences represent different magnetic mineralogies. Results for all three samples are similar in that they show a relatively smooth and gradual acquisition of the hard IRM without ever attaining saturation (Fig. 2), and relatively smooth thermal decay of the hard and medium IRM components with unblocking temperatures of 680 °C (Figs. 3A–3C). This suggests that the Willwood samples are dominated by the high-coercivity mineral hematite. We infer that the dominant carrier of the remanence magnetization in Willwood mudstones is fine-grained authigenic hematite formed during pedogenesis. One of the Willwood samples exhibited a significant soft IRM component that was largely unblocked by 580 °C (Fig. 3C), indicating the presence of minor amounts of magnetite or maghemite. Although Willwood mudstones often have yellowish mottles thought

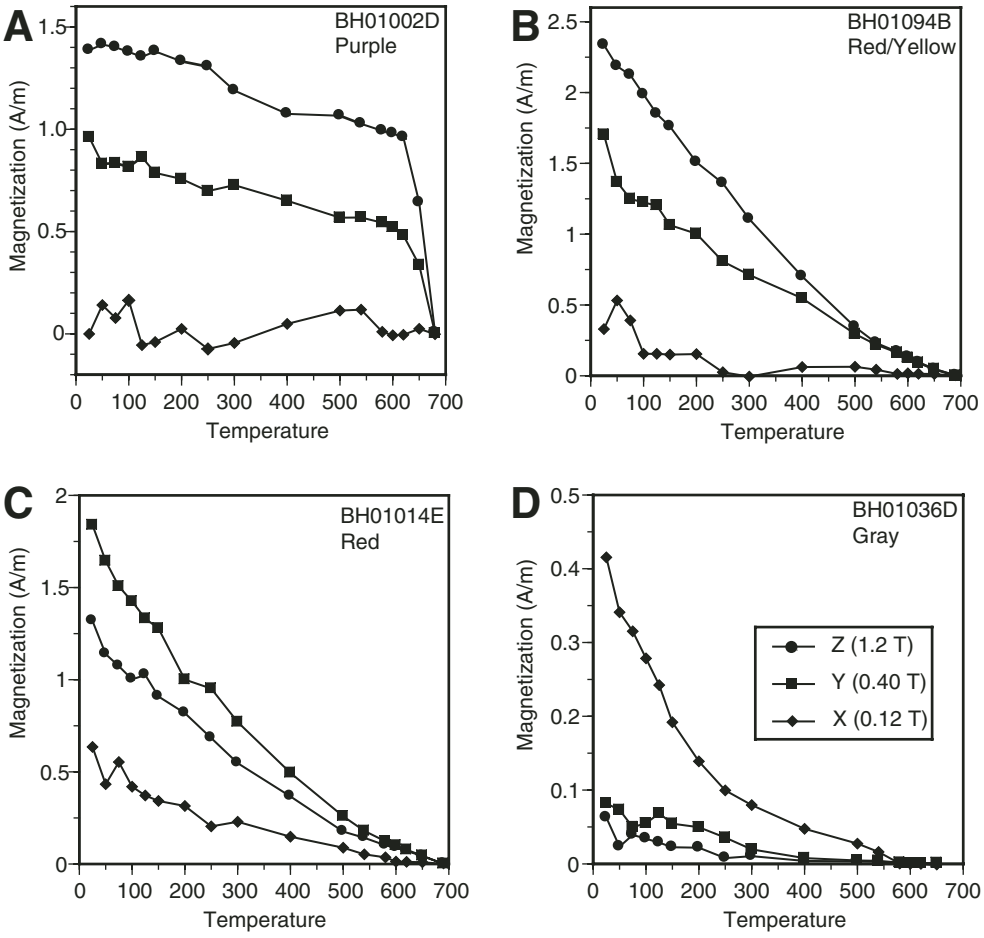

Figure 3. Thermal demagnetization of a three-axis isothermal remanent magnetization (IRM) for the same samples as shown in Figure 2 (see text for discussion of method). Willwood samples (A–C) show unblocking of dominant hard and medium IRM components at 690 °C, indicating hematite. The Fort Union sample (D) is dominated by the soft IRM component that unblocks at 580 °C, indicating magnetite. Symbol key for all diagrams is shown in D. *X* axis represents 0.12 T (diamonds), *Y* axis represents 0.40 T (squares), and *Z* axis represents 1.1 T (circles).

to be goethite (e.g., Kraus and Hasiotis, 2006), the presence of this mineral is not indicated by the IRM study of the yellow mottled sample BHIR094B (Fig. 3B).

The Fort Union sample (BHIR036D) exhibited distinctly different behavior during the IRM experiment. In this case, there was a rapid increase in intensity during the acquisition of IRM up to ~150 mT, after which the intensity reached a plateau (Fig. 2). Results of the three-axis IRM experiment indicated that the low-coercivity IRM was strongest and showed a gradual decrease in intensity during thermal demagnetization with final unblocking temperatures of 580 °C (Fig. 3D). Based on these results, magnetite seems to be the dominant carrier of remanent magnetization in Fort Union mudstones, and we suspect that it is detrital in origin.

Characteristic directions for the 42% of samples that exhibited linear decay to the origin were computed using least-squares analysis (Kirschvink, 1980; Figs. 4A–4C). Characteristic directions for the 23% of samples that showed initial decay followed by strong clustering of vector end points, but no linear decay to the origin, were calculated using a Fisher mean (Fig. 4D). In some samples (26%), the overlapping unblocking spectra of the magnetic components obscured any linear demagnetization trends, and we used the progression of remanence directions along a great circle path from the overprinting direction to a reversed characteristic direction (Fig. 4E). The rest of the samples (9%) exhibited unstable demagnetization behavior and could not be used for purposes of polarity determination (Fig. 4F).

Summary statistics were calculated for those sites that contained three samples exhibiting stable demagnetization. Alpha sites were those where all samples were characterized by a line or mean direction and the sample directions were significantly clustered according to the Watson (1956) test for randomness. Beta sites were those where all three samples exhibited consistent polarities, but one or more samples were characterized by a great circle direction. Individual samples that were not included in alpha or beta sites, but were still characterized by stable demagnetization, were also considered when interpolating between alpha or beta sites to define the bounds of polarity intervals.

Although the beds are only gently tilted, the mean characteristic directions from alpha sites show better clustering in stratigraphic coordinates (100% tilt correction) than geographic coordinates. Using the parametric bootstrapping method of Tauxe and Watson (1994), maximum clustering of mean directions for alpha sites occurs near 100% unfolding and the 95% confidence interval excludes 0% unfolding, ruling out a postfolding magnetization (Fig. 5; see GSA Data Repository Fig. DR1[1]). Although the mean characteristic directions for the alpha sites appear antipodal, they do not pass the reversal test at the 95% confidence level due to shallower reversed directions compared to the normal directions. This is likely a result of incomplete removal of present-day normal overprints from the reversed polarity samples. The overall mean characteristic direction (declination/inclination) for the alpha sites is 348/63 (α_{95} = 4.4), which agrees well with the expected direction of 349/63

[1]GSA Data Repository item 2007145, Figures DR1 and DR2, and Table DR1, are available at http://www.geosociety.org/pubs/ft2007.htm or by request to editing@geosociety.org.

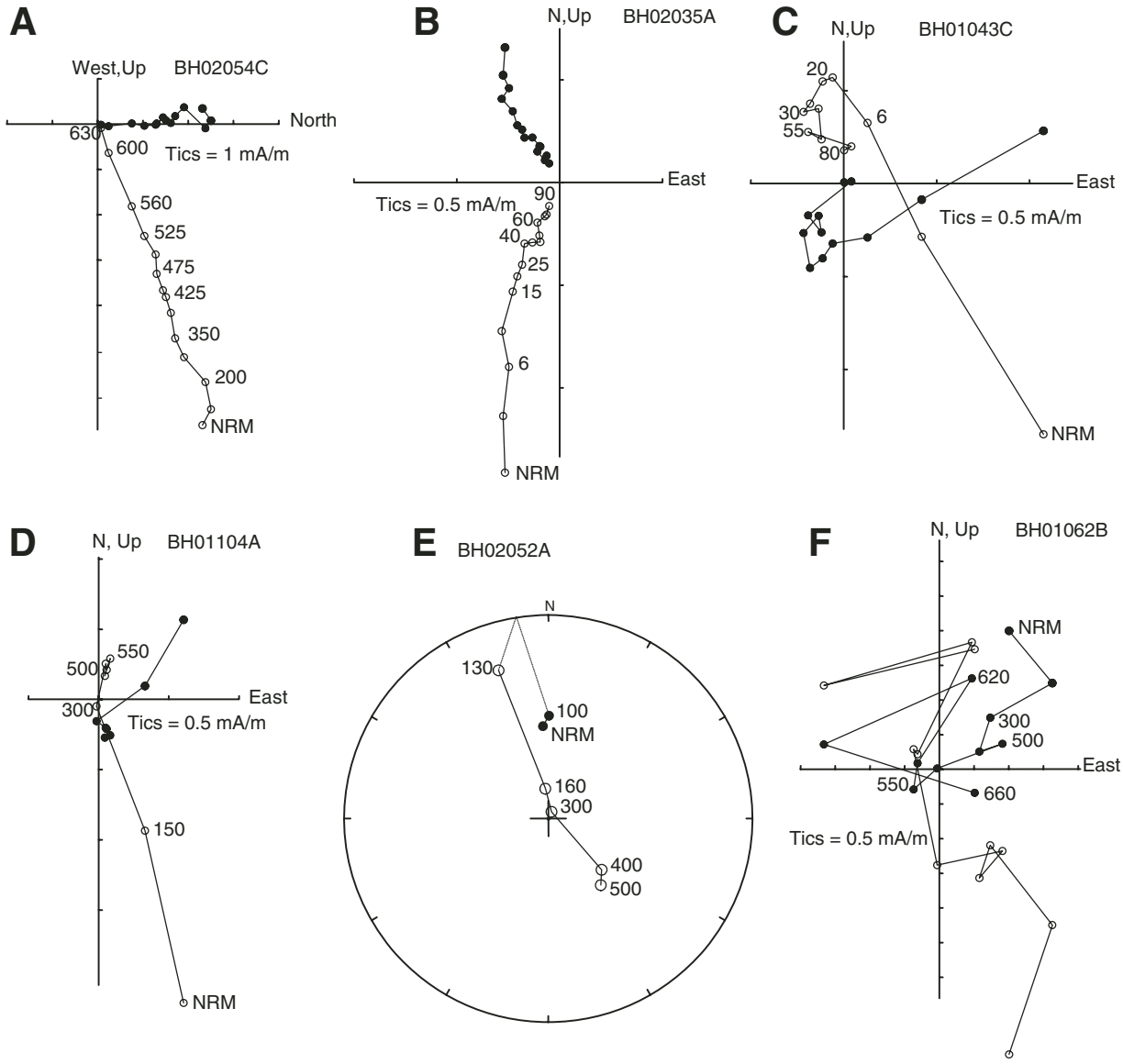

Figure 4. Representative demagnetization of samples from the Willwood (A, D, E) and Fort Union Formations (B, C, F) in the Bighorn Basin. Open symbols in Zijderveld (1967) diagrams (A–D, F) show vector end points in the vertical plane; closed symbols represent horizontal plane. Open symbols in equal-area projection (E) are on the upper hemisphere; closed symbols are on lower hemisphere. Samples are shown in tilt-corrected coordinates. NRM—natural remanent magnetization.

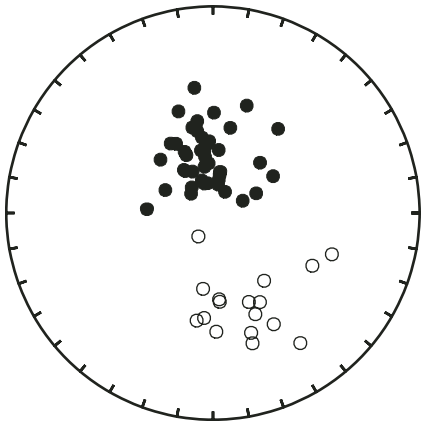

Figure 5. Equal-area projection of mean characteristic directions for alpha sites in tilt-corrected coordinates. The overall mean direction (declination/inclination) for the alpha sites is 348/63 (α_{95} = 4.4), almost identical to the expected direction of 349/63 (α_{95} = 2.6) for the early Eocene of the Bighorn Basin based on the Eocene reference pole for North America (Diehl et al., 1983), and is significantly different from the present geocentric axial dipole field direction of 0/63 for this location. Open symbols are on the upper hemisphere of the projection; closed symbols are on the lower hemisphere.

(α_{95} = 2.6) for the early Eocene of the Bighorn Basin based on the Eocene reference pole for North America (Diehl et al., 1983). The mean characteristic direction is also significantly different from the present geocentric axial dipole field direction for this location of 0/63.

MAGNETOSTRATIGRAPHIC RESULTS

Six different stratigraphic sections were sampled for this study. These sections were chosen to help resolve discrepancies from previous studies and fill stratigraphic and geographic gaps between previously sampled sections in the basin. When combined with previously reported magnetostratigraphic results, the polarity transitions in these sections complete a series of timelines that can be extended across much of the basin. This allows for most of the ~2225 fossil localities in the basin to be tied directly to a nearby magnetostratigraphic record. For the sake of completeness, results from each section are reported individually, and then the implications of this new basin-wide magnetostratigraphic framework are discussed. All summary statistics for paleomagnetic sample sites are listed in Table 1.

Fossil locality names that start with FG (Foster Gulch) are part of the University of Michigan Museum of Paleontology collection. Locality and faunal information for FG localities was reported in Clyde (1997) and has been archived in the Paleobiology Database (http://www.paleodb.org/). Fossil locality names that start with Y (Yale University collections) were described in Bown et al. (1994). Those starting with SLW (Scott L. Wing) and NMNH are part of the collections at the National Museum of Natural History (Smithsonian Institution).

Fort Union Formation

FG 47–48 Section

This 325-m-thick section of Fort Union Formation in Foster Gulch is ~3 km northwest of the Croc Tooth Quarry section of Secord et al. (2006), and extends through two late Tiffanian fossil localities (FG 47 and FG 48; Figs. 1 and 6). A carbonaceous shale bed was traced from the top of the Croc Tooth Quarry section to the 79 m level of the FG 47–48 section: Thirty-two paleomagnetic sites were sampled from this section and results indicate that there are 2 reversed polarity zones (A– and C–) and 2 normal polarity zones (B+ and D+) in the sequence. The bottom reversed polarity zone must be the same as the reversed polarity zone in the Croc Tooth Quarry section, based on lithostratigraphic correlation between these sections. Biostratigraphic data presented in Secord et al. (2006) indicate that this reversed polarity zone (A–) represents chron C26r. Zone B+ is interpreted to represent chron C26n, zone C– represents chron C25r, and zone D+ represents chron C25n.

FG 36–37 Section

The FG 36–37 section is 255 m thick, begins 1.2 km southeast of the top of the FG 47–48 section, and is stratigraphically directly above it (Figs. 1 and 6). The two localities at the base of this section (FG 36 and FG 37) represent either biostratigraphic zone Ti-6 or Cf-1, based on the presence of *Plesiadapis gingerichi* and *Carpolestes nigridens* at FG 37. This section has a normal polarity zone at its base overlain by a reversed polarity zone. The basal normal polarity zone correlates to zone D+ in the FG 47–48 section, based on a carbonaceous shale bed at the 320 m level of the FG 47–48 section that can be traced laterally to the 4 m level in the FG 36–37 section. This means that the reversed polarity zone in this section (zone E–) represents chron C24r and the reversal recorded in this section is the chron C25n-C24r boundary. The P-E boundary is recognized ~290 m above the top of this section, where it is associated with the lowest prominent red mudstone paleosol, the lowest occurrence of diagnostic Eocene mammalian taxa (e.g., *Hyracotherium*), characteristic Eocene floras, and a 6‰ carbon isotope anomaly (Clyde, 1997; Clyde and Gingerich, 1998; Koch et al., 2003).

Sand Creek Divide Section

The Sand Creek Divide section is 435 m thick and is ~70 km southeast of the Foster Gulch sections and ~15 km southeast of Manderson, Wyoming (Figs. 1 and 7). The section begins at what we interpret to be the Cretaceous-Tertiary (K-T) transition, which is unconformable in this area. Here, as in much of the southeastern Bighorn Basin, the Fort Union Formation is on an erosional surface developed on Upper Cretaceous strata of the Lance and Meeteetse Formations. The Sand Creek Divide section ends at a thick red paleosol in the Willwood Formation that is characteristic of the late phase of the Paleocene–Eocene Thermal Maximum (PETM) in the southeastern Bighorn Basin. Evidence supporting the placement of the P-E boundary at the top of this section includes a carbon isotope excursion preserved in pedogenic carbonate nodules (Koch et al., 1995), the presence of Wasatchian-0 mammals (Smith et al., 2006), and the lack of extensive red mudstone paleosols below this level. No identifiable fossil mammals have yet been recovered from the Paleocene deposits of the Sand Creek Divide area despite excellent exposures: this is probably due to limited collection effort. Fossil plant localities are relatively abundant in this area and several of these are in this section (Fig. 7). The fossil floras are dominated by *Cercidiphyllum*, *Metasequoia*, *Trochodendroides*, *Macginitiea*, and other typical late Paleocene plants. No previous paleomagnetic studies have been done on the Fort Union Formation in the southern part of the basin, so the results presented here provide new temporal data on the initiation of basin development in this region. The section is dominantly reversed polarity (zone G– and I–) with an ~40 m normal polarity zone at the base (zone F+) and another normal polarity zone between ~170 and 240 m (zone H+). The single normal polarity alpha site at 90 m may represent a cryptochron (a minor magnetic anomaly on the seafloor that can be correlated between records and represents a short-term variation in the polarity and/or intensity of the geomagnetic field; Cande and Kent, 1992a, 1992b) or an unremoved present-day normal overprint (see following). Because the P-E boundary is at the top of this section, we correlate zone I– to chron C24r. Assuming stratigraphic completeness, zone H+ likely represents chron C25n, zone G– represents chron C25r, and F+ represents chron C26n.

Willwood Formation

Antelope Creek Section

This section is 290 m thick and begins ~3 km southwest of Basin, Wyoming, in a thick red paleosol that correlates lithostratigraphically to the top of the Sand Creek Divide section, and marks the P-E boundary in this region (Figs. 1 and 8). For sake of consistency, we referenced our samples to the section of Schankler (1980), who also tied in most of the fossil localities in the area. The fossil localities that are directly along the line of section that we sampled are shown in Figure 8. Localities from this section are within the *Haplomylus-Ectocion* Range Zone of Schankler (1980), essentially equivalent to fossil mammal zones Wa-1–Wa-4 of Gingerich (1991). Fossil plants in the basal 120 m of the section include Eocene indicators such as *Lygodium*, *Cnemidaria*, *Salvinia*, and abundant leaves of *Alnus* (Wing et al., 1995). Pollen samples from the same beds document the local first appearances of *Platycarya* and *Intratriporopollenites instructus* (Wing and Harrington, 2001), which are widely recognized Eocene index fossils. This section is entirely characterized by reversed polarity, except for a single alpha site of normal polarity at the top of the section. Because this section begins at the mature paleosol horizon marking the P-E boundary, the reversed polarity interval (zone J–) correlates to the reversed polarity zone at the top of the Sand Creek Divide section (zone I–), and thus is

Figure 6. Magnetostratigraphic sections in the Fort Union Formation of Foster Gulch. Cedar Point Quarry section and Croc Tooth Quarry section are from Secord et al. (2006). FG 47–48 and FG 36–37 sections are from this study. Widths of lithological beds represent grain size as shown in key, whereas the shading represents color. Vertebrate fossil localities are listed to right of lithological sections; biostratigraphic zones are indicated when known. CPQ—Cedar Point Quarry, DQ—Divide Quarry, CTQ—Croc Tooth Quarry. FG localities are from Foster Gulch (University of Michigan Museum of Paleontology). VGP Lat is virtual geomagnetic pole latitude; circles in paleomagnetic data represent mean characteristic directions for alpha sites, squares represent mean characteristic directions for beta sites, and small crosses represent characteristic directions of individual samples from other sites. Lettered zones at right (e.g., A–) are local polarity zones. Preferred correlation of local polarity zones to the geomagnetic polarity time scale is indicated by the chron (e.g., C26R) listed under each local zone. Short normal polarity event in zone C (C25R) may be a cryptochron.

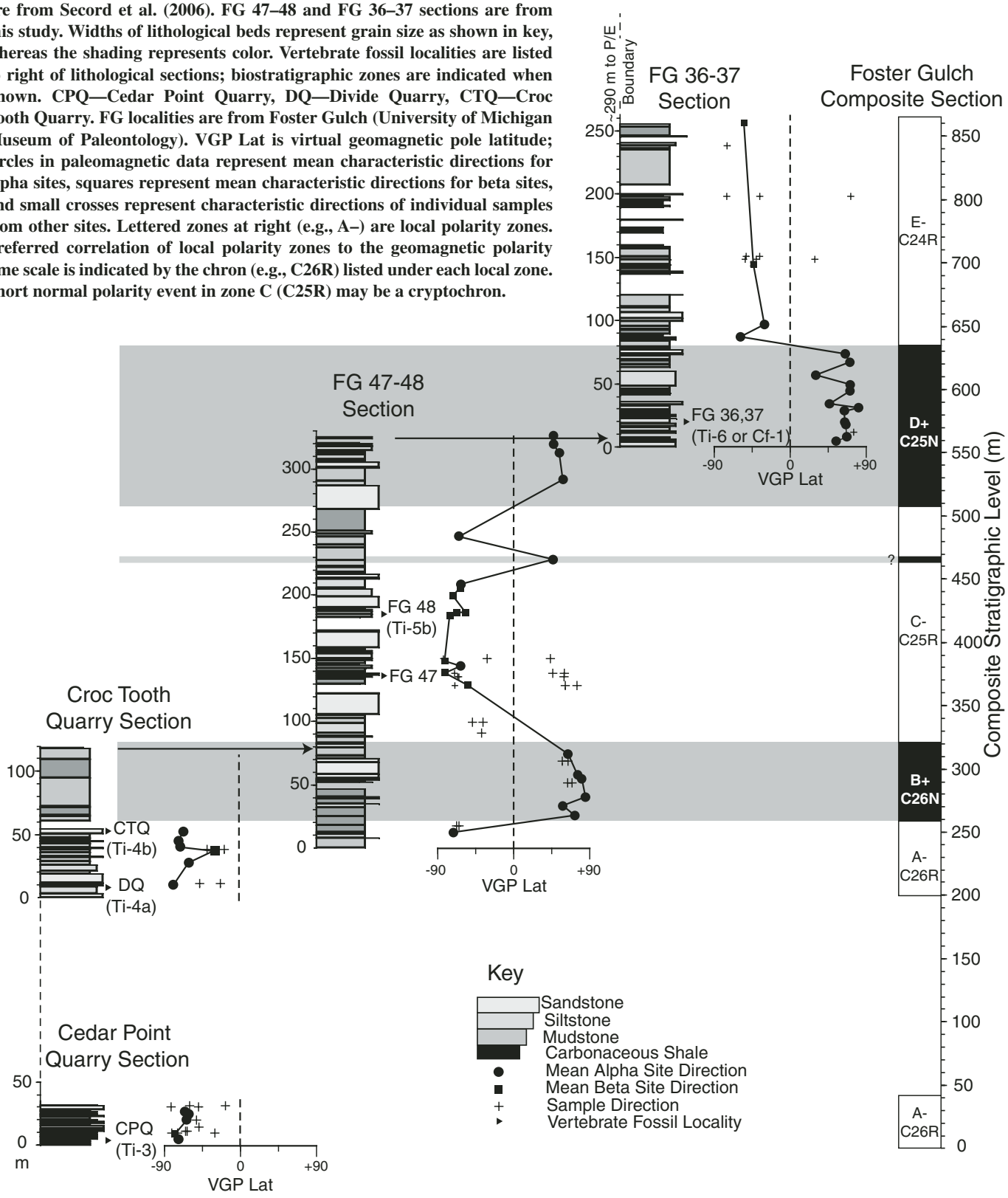

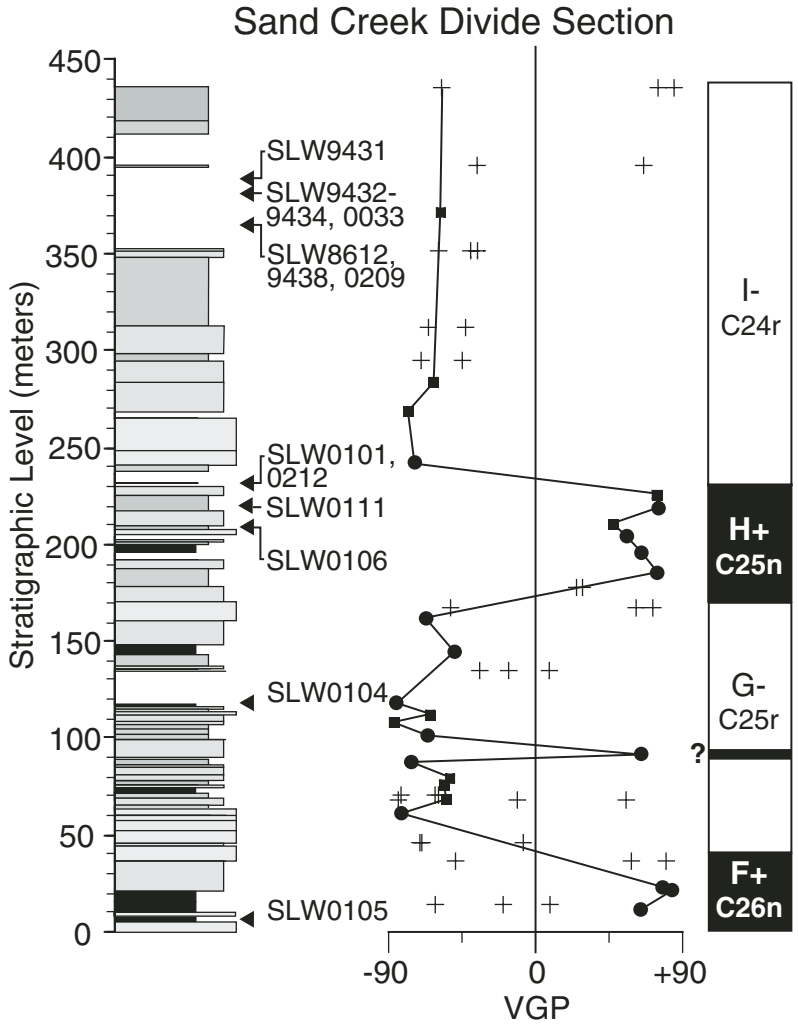

Figure 7. Magnetostratigraphy of Sand Creek section in the Fort Union Formation from the central Bighorn Basin. Width of lithological beds represents grain size as shown in key of Figure 6, whereas the shading represents color. Plant fossil localities are listed to right of lithological sections. Fossil locality names that start with SLW (Scott L. Wing) are part of the collections at the National Museum of Natural History (Smithsonian Institution). VGP Lat is virtual geomagnetic pole latitude; circles in paleomagnetic data represent mean characteristic directions for alpha sites, squares represent mean characteristic directions for beta sites, and small crosses represent characteristic directions of individual samples from other sites. Lettered zones at right (e.g., I–) are local polarity zones. Preferred correlation of local zones to the geomagnetic polarity time scale is indicated by the chron (e.g., C24R) listed under each local zone. Short normal polarity event in zone G (C25R) may be a cryptochron.

interpreted to represent chron C24r. On the basis of lithostratigraphic correlation to the adjacent Dorsey Creek section, we interpret the single normal site at the top of the section to be either an unremoved present-day normal overprint or a cryptochron within chron C24r (see following).

Dorsey Creek Section

The base of the 225-m-thick Dorsey Creek section is ~5.5 km southeast of Otto, Wyoming and ~14.5 km west of Basin, Wyoming (Figs. 1 and 8). The section begins ~20 m below locality Y-286 within the upper *Haplomylus-Ectocion* Range Zone in beds that correlate to the upper part of the Antelope Creek section. The section ends at the top of a large bluff (informally referred to as Granger Ridge) that rises steeply behind locality Y-152. Locality Y-421, which is one of the lowest localities within the *Bunophorus* Interval Zone of Schankler (1980), is just west of the section line and was traced to the 140 m level of the section. Fossil plants from locality USNM37656 (SLW0130 and SLW0131) in this section document the coolest climates of the early Eocene in the Bighorn Basin (Wing et al., 1991, 2000; Fig. 8).

Results from the 45 paleomagnetic sites sampled from this section indicate that the section is predominantly reversed polarity with a change to normal polarity at the ~200 m level. We correlate the lower reversed polarity interval of this section to the reversed polarity interval of Antelope Creek (zone J–) on the basis of their stratigraphic overlap, and therefore interpret them to correspond to chron C24r. We correlate the upper normal polarity zone (zone K+) to chron C24n.3n, consistent with the results of Clyde et al. (1994), who found the first appearance of *Bunophorus* (Wa-4–Wa-5 zone boundary) and Biohorizon B just below the chron C24r-C24n transition. There are two isolated normal polarity sites within zone J– in the Dorsey Creek section. We interpret these as either present-day normal overprints or cryptochrons (see following).

Elk Creek Rim Section

The Elk Creek Rim section is 25 km southwest of Basin, Wyoming, and begins ~15 m stratigraphically below fossil locality Y-127 (Figs. 1 and 8). Biohorizon B, which separates the upper *Haplomylus-Ectocion* Range Zone from the *Bunophorus* Interval Zone and also approximates the Wa-4–Wa-5 zone boundary, is very close to the base of this section, although its precise placement is uncertain due to poor paleontological sampling in the lower most part of the section. The section is 130 m thick and ends just above fossil locality Y-126U. (There are two Y-126 localities, one at the top of Elk Creek rim, which we refer to here as Y-126U, and one at the bottom of the rim, which we refer to as Y-126L; see Bown et al. [1994, p. 99] for an explanation.)

Fossil plants from near YPM-127 (plant locality USNM37661) give the earliest paleobotanical indications of a renewed increase in temperature following the earliest Eocene cool period, and this warming trend is strongly indicated by floras collected at locality USNM37560 (SLW905–907) from near the top of the section (Wing et al., 2000).

We sampled 18 paleomagnetic sites from this section. Results indicate that the bottom 30 m is reversed polarity and the upper 70 m is normal polarity, the intervening 30 m being mixed polarity. This interval of mixed polarity is problematic because it contains a close succession of samples with differing polarity and it separates an interval of consistently reversed polarity below from an interval of consistently normal polarity above (Fig. DR2; see footnote 1). This noisy polarity pattern could be due to

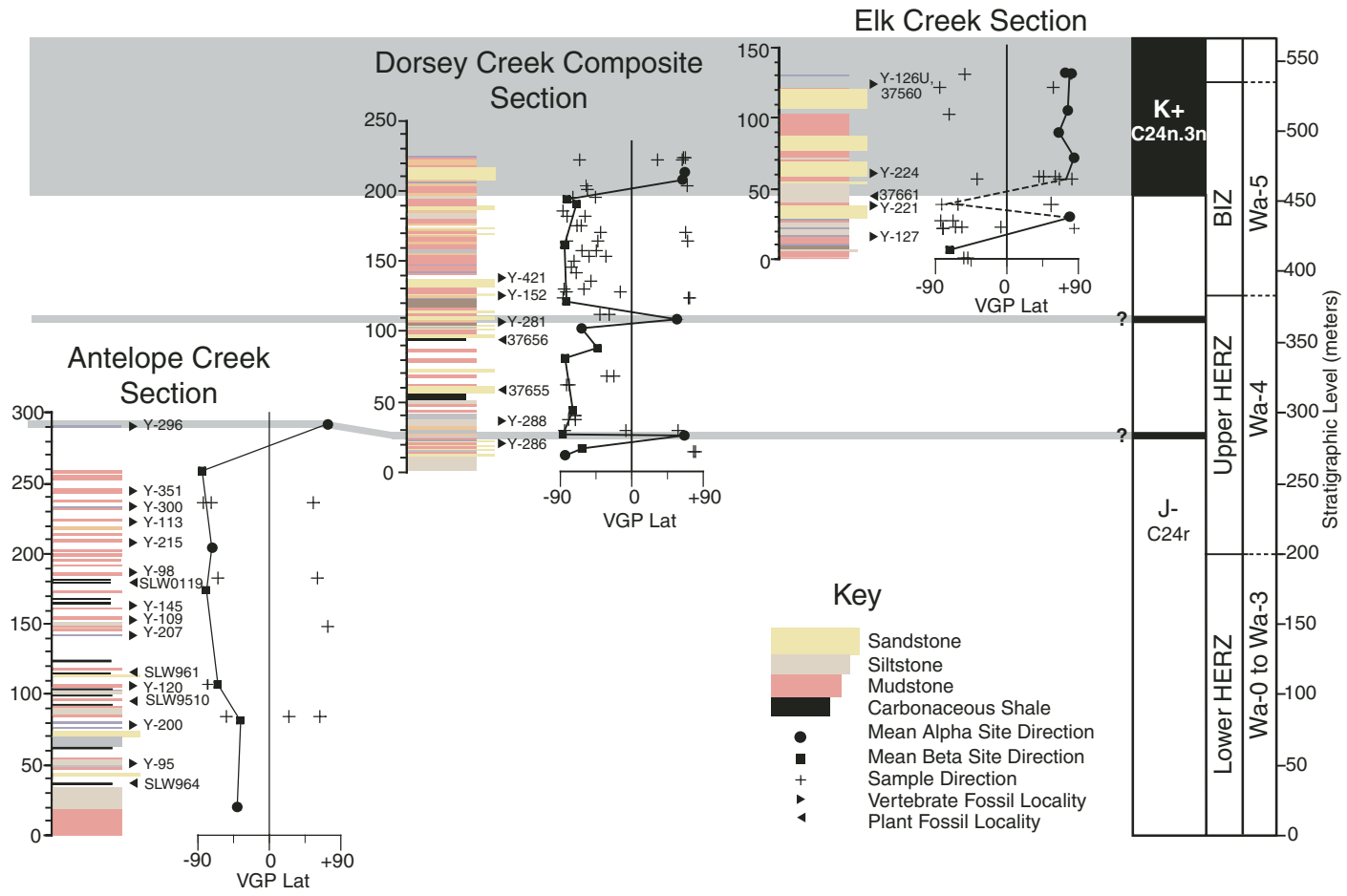

Figure 8. Magnetostratigraphic sections in the Willwood Formation from the central Bighorn Basin. Widths of lithological beds represent grain size, as shown in key, whereas the shading represents color. Plant and vertebrate fossil localities are listed to the right of lithological sections. Fossil locality names that start with Y are part of the Yale University collections; those starting with SLW and 37 (NMNH) are part of the collections at the National Museum of Natural History (Smithsonian Institution). VGP Lat is virtual geomagnetic pole latitude; circles in paleomagnetic data represent mean characteristic directions for alpha sites, squares represent mean characteristic directions for beta sites, and small crosses represent characteristic directions of individual samples from other sites. Lettered zones at right (e.g., J–) are local polarity zones. Preferred correlation of local polarity zones to the geomagnetic polarity time scale is indicated by the chron (e.g., C24R) listed under each local zone. Short normal polarity events in zone J (C24R) may be cryptochrons. HERZ—*Haplomylus-Ectocion* Range Zone (Schankler, 1980), BIZ—*Bunophorus* Interval Zone (Schankler, 1980). Wa 0-5—biostratigraphic zones of Gingerich (1991).

real variations in the geomagnetic field during the reversal, heterogeneous rates of remanent magnetization lock-in, or a currently unrecognized stratigraphic feature that complicates local superposition (e.g., a mud-filled channel). If we assign the reversal to the middle of this poorly defined polarity interval, then it corresponds to the ~450 m level of the Schankler composite section, which agrees closely with the level of the chron C24r-C24n reversal in the Dorsey Creek section (455 m level in the Schankler composite section). This suggests that the dominant polarity reversal recorded in the Elk Creek Rim section represents the chron C24r-C24n reversal. It is important to note that no matter where the reversal is placed within the 30 m of mixed polarity, it is still well above the projected level of Biohorizon B in this section (Fig. 8).

DISCUSSION

Intrabasinal Correlations and Biotic Implications

The new magnetostratigraphic framework for the Bighorn Basin provides a series of timelines that can be traced across the entire basin, making it possible to correlate fossil localities from distant parts of the basin into a single chronostratigraphy (Fig. 9). Although previous studies have developed chronostratigraphic frameworks for particular localized parts of the basin, it has been difficult to correlate these local frameworks to each other due to different biostratigraphic zonations, imprecise biostratigraphic data, and very different stratigraphic thicknesses. For example, Schankler (1980) identified a period of significant faunal reorganization at the 380 m level in his Elk Creek composite section and named it Biohorizon B. Biohorizon B is characterized by the local extinction of 13 species, 6 of which are also generic extinctions (e.g., *Haplomylus* and *Ectocion*), and it defines the lower limit of Schankler's *Bunophorus* Interval Zone. Biohorizon B coincides closely with the beginning of Gingerich's (1983) zone Wa-5, although the latter is defined explicitly by the first appearance of *Bunophorus*, which typically coincides with Biohorizon B but has also been reported from a few specimens below that level in the 15-Mile

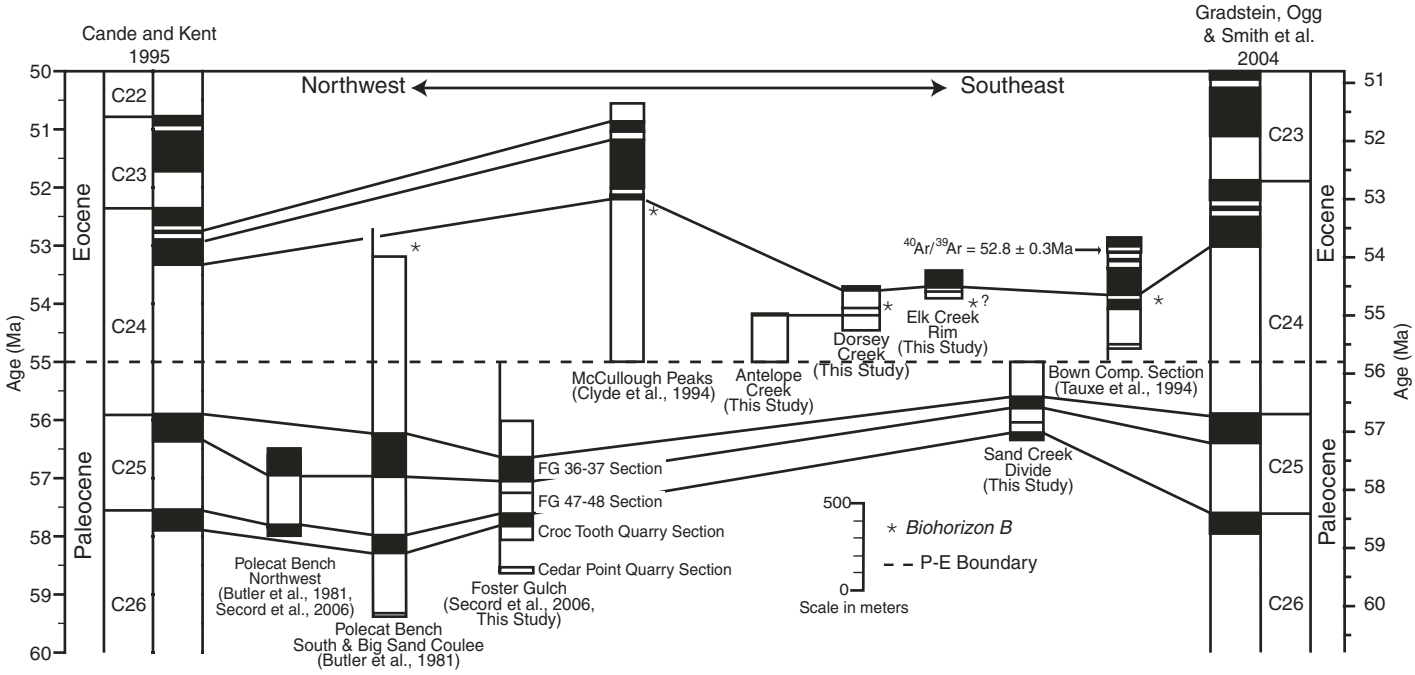

Figure 9. Magnetostratigraphic correlation across the Bighorn Basin, Wyoming. The Paleocene-Eocene (P-E) boundary is marked by the dashed line and forms the datum for fence diagram. Asterisk shows stratigraphic level of Biohorizon B (~Wa-4–Wa-5 zone boundary). Note that the chron C24r-C24n boundary is stratigraphically above Biohorizon B in all sections except southern Bighorn Basin composite section sampled by Tauxe et al. (1994).

Creek area. During initial paleomagnetic investigations in the McCullough Peaks region of the basin, Clyde et al. (1994) found Biohorizon B and the first occurrence of *Bunophorus* ~100 m stratigraphically below a normal polarity zone (their zone C+) that was interpreted to be the base of chron C24n.3n. Tauxe et al. (1994) sampled the composite section of Bown et al. (1994) in the southern part of the basin and found this same biotic event ~60 m above a normal polarity zone (their zone N2) that they interpreted to be the base of chron C24n.3n. This discrepancy not only produced considerable uncertainty about the age of this important faunal turnover, but also created confusion regarding the age and relative magnetostratigraphic placement of the P-E boundary as defined by the carbon isotope excursion (CIE). Our new results from the central part of the basin, particularly from Dorsey Creek where the biostratigraphy and magnetostratigraphy are best delimited, show that the key biostratigraphic events associated with Biohorizon B, including the first appearance of *Bunophorus*, occur below chron C24n.3n.

We interpret polarity zone N2 of Tauxe et al. (1994) to be a normal overprint or merged cryptochrons, implying that zone N3 in that study marks the beginning of chron C24n.3n. Interpreted this way, all available stratigraphic sections in the basin for which there are relevant results show the same superpositional pattern of biostratigraphic and magnetostratigraphic events through this interval. The problematic polarity zone N2 from Tauxe et al. (1994) was sampled from strata along 15-Mile Creek, ~25 km south of Elk Creek Rim and a similar distance from where they sampled polarity zones R3 and N3 (Fig. 1). Although zone N2 is defined by three alpha sites, one of those sites has an intermediate direction and individual samples exhibit a mixture of polarities (see Fig. 4 of Tauxe et al., 1994). Sediment accumulation rates are considerably lower in the southern part of the basin compared to the north, resulting in more mature paleosols in the south. These mature paleosols in the southern basin may be more prone to present-day normal polarity overprints or to shallow burial overprinting by chron C24n during the Eocene. It is also possible that the slower accumulation rates are caused by more pronounced hiatuses and that zone N2 represents a composite record of two (or more) cryptochrons with no sampling of the intervening reversed polarity intervals. The interpretation of cryptochrons as full polarity changes of the geomagnetic field, however, remains controversial (see discussion in Acton et al., 2006). In either case, this interpretation argues that the 15-Mile Creek strata associated with Tauxe et al. (1994) polarity zone N2 are correctly correlated into the broad composite section of Bown et al. (1994), but that the polarity is a product of either overprinting or compositing of short normal events within chron C24r. Alternatively, it is possible that zone N2 strata record the onset of chron C24n, but are incorrectly correlated to the composite section. If this were true, we would expect the fauna from zone N2 strata to be post–Biohorizon B (e.g., *Bunophorus* Interval Zone, Wa-5); however, there are numerous occurrences of *Haplomylus* and *Ectocion* in the 15-Mile Creek localities where zone N2 was sampled, and both taxa disappear at Biohorizon B in all other sections.

These new paleomagnetic data are also relevant to an ongoing discrepancy between the Schankler (1980) and Bown et al. (1994) composite sections that has caused considerable confusion over how the Elk Creek fossil localities correlate to localities farther south (e.g., those along 15-Mile Creek). Even though both sections begin at the P-E boundary, localities at the base of Elk Creek Rim (e.g., Y-127) are reported to be ~30 m lower in the Bown section than in the Schankler section, whereas localities above the Elk Creek Rim (e.g., Y-227) are reported to be ~70 m lower in the Bown section than in the Schankler sections. Our new results highlight this discrepancy. In our Dorsey Creek section, the level of the chron C24r-C24n polarity reversal corresponds to the ~455 m level in both the Bown composite section and the Schankler section. In the Elk Creek Rim section, the paleomagnetic data are not as clear, but show that

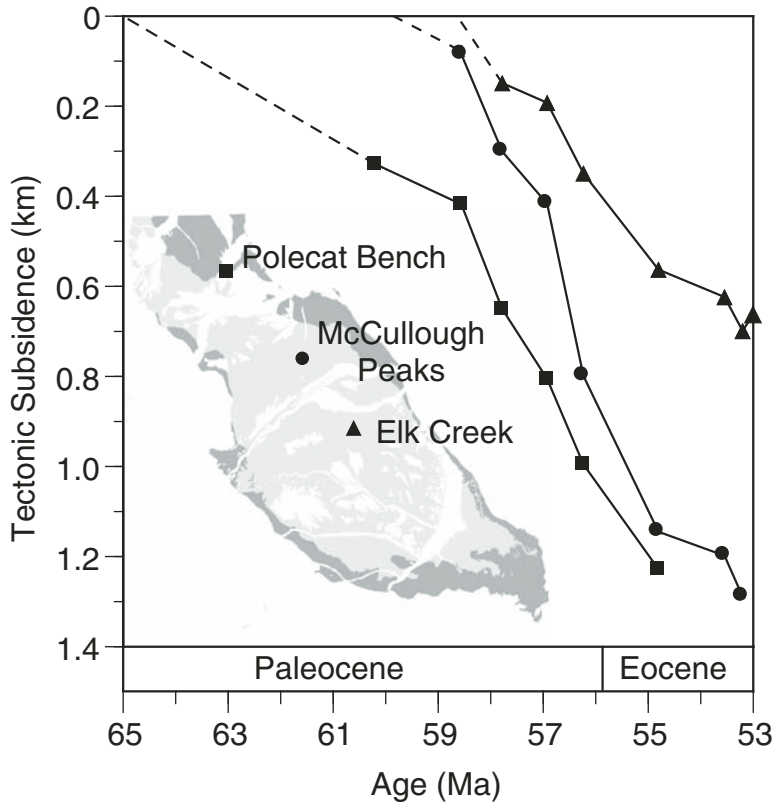

Figure 10. Tectonic subsidence (uncompacted thickness – passive subsidence) as calculated from backstripping analysis for three different parts of the basin. From northwest to southeast, the sections are Polecat Bench (squares), McCullough Peaks (circles), and Sand Creek–Elk Creek (triangles). Note that tectonic subsidence initiated in the northwestern part of the basin near the Beartooth uplift and proceeded in a time-transgressive sense to the southeast. Rates of tectonic subsidence (slope of lines) were also greater in northern part of the basin compared to southern part of the basin.

the level of the same reversal corresponds to the ~400–430 m level in the Bown section and to the ~435–465 m level in the Schankler section. There are two likely reasons for this difference in composite levels. First, differences in measurement of the Elk Creek Rim section may be due to errors incurred during measurement with a Jacob staff. Second, there may be real differences in the thickness of the lower section along 15-Mile Creek, where Bown measured it, compared to the thickness of the lower section along Elk Creek, where Schankler measured it. The Elk Creek section being somewhat thicker than the 15-Mile Creek section would not be surprising given its more northern position and the northwest-southeast asymmetry in sediment accumulation rates (Gingerich, 1983; see following discussion).

Given the internal consistency of the stratigraphic position of the chron C24r-C24n polarity reversal relative to the Schankler section, we suspect that the Elk Creek Rim localities are somewhat miscorrelated in the Bown composite section. Bown et al. (1994) listed locality Y-127 at the 390 m level, whereas Schankler (1980) listed it at the 420 m level; however, both studies place Biohorizon B at a level of ~380 m. Thus, Bown et al. (1994) would place Biohorizon B only ~10 m below locality Y-127, whereas Schankler (1980) would place it ~50 m below that locality. According to Bown et al. (1994), locality Y-126L is ~20 m below Y-127, which implies that it should contain a post–Biohorizon B fauna according to the Schankler section, but a pre–Biohorizon B fauna according to the Bown section. Unfortunately, this locality is currently too poorly sampled to reliably classify its fauna and resolve this issue.

On the basis of our data, the most logical solution to this ongoing stratigraphic discrepancy is to separate the Elk Creek section of Schankler (1980) from the rest of the composite section of Bown et al. (1994). Localities in the Elk Creek area (sections AC-AC', EC-EC', SFE-SFE', DC-DC', ECW-ECW' from Bown et al., 1994, Table 16 and Plate 1) should no longer be referenced to the Bown et al. (1994) composite section but, instead, to the original Schankler (1980) section. Because the two sections converge at Elk Creek Rim (sections ER-ER' and ECR-ECR' in Bown et al., 1994), all fossil localities from this level and higher have been correlated to both sections, and are assigned two different stratigraphic levels, one from the Bown composite section and one from the Schankler section.

When stratigraphic data from the McCullough Peaks (Clyde et al., 1994), Dorsey Creek (this study), and Elk Creek Rim (this study) are considered, and all of the uncertainties relative to the Elk Creek Rim section are incorporated, Biohorizon B is 20–100 m below the chron C24r-C24n reversal. Using section-specific sediment accumulation rates, this translates into Biohorizon B occurring 100–220 k.y. before the chron C24r-C24n reversal. A short-term carbon isotopic anomaly called Elmo that is similar to, but of lower amplitude than, the CIE at the P-E boundary has been identified 1–2 m below chron C24n in deep-sea sediment cores collected during Ocean Drilling Program Leg 208 (Lourens et al., 2005). That study also interpreted increased carbon isotopic variability below chron C24n in a composite record of previously published Bighorn Basin data to be a terrestrial record of this same Elmo event (see Lourens et al., 2005, supplementary Fig. 6). The putative Bighorn Basin Elmo of Lourens et al. (2005) is particularly important because it represents the only evidence of strong links between marine and terrestrial biogeochemical cycling similar to those documented for the higher amplitude CIE at the P-E boundary. However, the correlation of Elmo to the Bighorn Basin record is complicated by two factors: (1) recent high-resolution sampling through this interval at Dorsey Creek recovered no clear carbon isotope anomaly (see Clyde et al., 2006), and (2) the marine record lacks a precise temporal model for this time interval because of significant dissolution at both the PETM and Elmo events. Despite these uncertainties, the new magnetostratigraphic data presented here make it clear that both Biohorizon B and Elmo occurred within ~250 k.y. of the chron C24r-C24n reversal. A precise determination of whether these two events coincide will remain difficult until the marine chronostratigraphy of this interval is better defined and a clear isotopic record of Elmo is recovered from a Bighorn Basin section in which Biohorizon B is well defined.

Origin of Short Normal Polarity Events

Several short normal polarity events were found within our record of chrons C24r and C25r. These normal polarity events are

interpreted to be either cryptochrons or strong normal polarity overprints. Cryptochrons are minor magnetic anomalies on the seafloor that can be correlated between records and represent short-term variations in the polarity and/or intensity of the geomagnetic field (Cande and Kent, 1992a, 1992b). Although the exact nature of cryptochrons remains controversial, at least some appear to represent full polarity reversals of the geomagnetic field that could imprint continental sedimentary strata (Acton et al., 2006). Chrons C24r and C25r are characterized by 16 different cryptochrons (Cande and Kent, 1992a), so it is possible that some of the isolated normal polarity sites found in the Bighorn Basin during this interval represent these. This interpretation is supported by the observation that one of the short normal polarity events in the Willwood Formation seems to correlate between adjacent sections (Fig. 8). Given the short duration of cryptochrons and the inherent incompleteness of fluvial stratigraphic sequences like the ones studied here, their inconsistent appearance in these sections would be expected (see Roberts and Winklhofer, 2004). However, the prevalence of these normal polarity events seems to increase toward the south of the basin, where sediment accumulation rates are lowest and paleosols are most mature. This suggests that these normal polarity sites may be related to mineralogical differences, pointing to the possibility of present-day overprints. Overprints are common in Willwood samples and sometimes difficult to remove entirely during demagnetization. The single Fort Union example of an isolated normal polarity event (Fig. 7) is more noteworthy, because these facies appear to be significantly less susceptible to present-day overprints as compared to the Willwood paleosols. Unfortunately, the present-day field direction in the Bighorn Basin is so similar to the Eocene direction that it is difficult to conclusively distinguish a normal polarity overprint component from a normal polarity Eocene component when secular variation is taken into account. A focused paleomagnetic study of these isolated normal polarity sites will be required to fully understand their origin.

Tectonic Evolution of the Bighorn Basin

The Bighorn Basin is an intermontane basin that formed in flexural response to loading of adjacent Laramide uplifts (Bighorn Mountains, Beartooth Mountains, and Owl Creek Mountains). Our new magnetostratigraphic framework provides temporal and spatial constraints on the pattern of sediment accumulation that help illustrate the structural evolution of the basin. One way to evaluate this information is to use a local backstripping model like that employed by Steckler and Watts (1978). Backstripping is a numerical method that uses an observed stratigraphic record to estimate the depth to basement in the absence of sediment and water loading. This depth is a measure of the active subsidence caused by tectonic and/or thermal forces. By applying this approach to progressively older time steps, it is possible to distinguish the relative importance of passive and active subsidence during the formation of a particular sequence of basin fill.

Backstripping curves for the period of Laramide-style Bighorn Basin development were constructed using the local loading model originally outlined by Steckler and Watts (1978) and further detailed in Watts (2001, p. 309–315). This one-dimensional model assumes pure Airy isostasy in estimating the amount of active subsidence necessary to account for a given thickness of sediment. It does this by first estimating the uncompacted thickness of a given stratigraphic sequence for a particular time interval, and then subtracting the passive subsidence expected from sediment and water loading. With no marine facies in our stratigraphic sections, the water depth and sea-level terms are dropped from the classic backstripping equation (equation 7.9 in Watts, 2001), leaving only the saturated-sediment loading term. Therefore,

$$Y_i = S^*_i \left[\frac{\rho_m - \bar{\rho}_{si}}{\rho_m - \rho_w} \right], \quad (1)$$

where Y_i is active subsidence at time i, S^*_i is uncompacted thickness at time i, ρ_m is the mantle density (assumed to be 3330 kg/m^3), ρ_w is the density of water (1000 kg/m^3), and $\bar{\rho}_{si}$ is the mean density of uncompacted sediment at time i. Both unknowns, S^*_i and $\bar{\rho}_{si}$, are determined at each time step by using a porosity-depth model because both variables are strongly related to porosity (see Watts, 2001; Table DR1 [see footnote 1]). No down-core porosity data are available from the Bighorn Basin deposits studied here, so our porosity-depth model relies on published data from other settings and takes the exponential form of

$$\Phi = 0.62 \quad e^{-z\ 0.43}, \quad (2)$$

where Φ is porosity and z is depth in kilometers. The initial (uncompacted) porosity of 0.62 was determined by applying the porosity-grain size relationship of Wu and Wang (2006) to an estimate of the typical grain size distributions for the Fort Union and Willwood Formations. These typical grain size distributions were based on stratigraphic sections in this paper and elsewhere (e.g., Kraus, 1997; Clyde and Christensen, 2003). The depth constant (0.43) is intermediate to the shale and sandstone values presented in Kominz and Pekar (2001). The porosity-depth model contributes the most uncertainty to the backstripping analysis. Although this uncertainty affects the absolute magnitude of subsidence estimates, it does not affect our comparison of subsidence patterns between sections, because the porosity-depth relationship is unlikely to differ significantly between sections. Our subsidence calculations do not account for likely postdepositional (i.e., post–early Eocene) burial (McMillan et al., 2006), which means they represent minimum estimates; however, this should not substantially affect the relative comparisons we focus on here. Cretaceous deposits in the Bighorn Basin predate Laramide partitioning of the Rocky Mountain foreland in this region, and were assumed to be fully compacted, so were treated as the basement rock for this analysis. Detailed calculations of this backstripping analysis can be found in Table DR1; see footnote 1.

The backstripping results show that tectonic subsidence was greatest in the northwest part of the basin and was least in the southeast part of the basin (Fig. 10). This was largely due to basin formation initiating in the northwestern portion of the basin and then proceeding to the southeast. Evidence of the time-transgressive nature of basin initiation is found in the conformable Lance (Cretaceous)–Fort Union (Paleocene) contact on Polecat Bench, an unconformity between Lance Formation and chron C26r in the Fort Union Formation at Foster Gulch, and an unconformity between Lance Formation and chron C26n in the Fort Union Formation at Sand Creek Divide. Although this difference in the timing of basin onset accounts for the majority of geographic asymmetry in Cenozoic subsidence in the Bighorn Basin, there is also significant asymmetry in subsidence rates (Fig. 10). For example, the average tectonic subsidence rates over the study interval are ~200 m/m.y. at Polecat Bench and ~250 m/m.y. at McCullough Peaks, but only ~85 m/m.y. in the southern Bighorn Basin. The earlier onset of basin development and higher rates of tectonic subsidence in the northwestern part of the basin, compared to the southeastern part of the basin, suggest that the loading of the Beartooth uplift played a dominant role in basin formation.

CONCLUSIONS

New and old magnetostratigraphic data from the Bighorn Basin are integrated into a basin-wide chronostratigraphic framework. Fossil localities from distant parts of the basin can

now be precisely correlated to one another using information that is independent of the fossils. Previous uncertainties associated with the timing of Biohorizon B, which is the single largest faunal turnover in the early Eocene record from the Bighorn Basin, are now resolved. The faunal turnover associated with Biohorizon B occurs stratigraphically below the chron C24r-C24n.3n polarity reversal, and may correspond to the Elmo isotopic event in the marine record. Several short normal polarity events are recognized in Bighorn Basin records of chrons C24r and C25r. These short events could represent cryptochrons; however, normal polarity overprints cannot be ruled out. Spatial and temporal patterning of tectonic subsidence as illustrated through backstripping indicates that the asymmetry of Bighorn Basin deposition is the result of both time-transgressive northwest to southeast initiation of basin formation and a geographic difference in tectonic subsidence rates.

ACKNOWLEDGMENTS

We thank P. Gingerich, K. Rose, J. Clark, and A. Wood for helpful discussions and assistance with field work. L. Gannon, J. Cristallo, M. Eller, B. Dawley, B. Plis, and M. Power helped with lab work. Ross Secord, Barry Albright, and an anonymous reviewer provided valuable comments on the manuscript. This research was funded in part by National Science Foundation grant EAR-0001379.

REFERENCES CITED

Acton, G., Guyodo, Y., and Brachfeld, S., 2006, The nature of a cryptochron from a paleomagnetic study of Chron C4r.2r recorded in sediments off the Antarctic Peninsula: Physics of the Earth and Planetary Interiors, v. 156, p. 213–222, doi: 10.1016/j.pepi.2005.09.015.

Bown, T.M., Rose, K.D., Simons, E.L., and Wing, S.L., 1994, Distribution and stratigraphic correlation of upper Paleocene and lower Eocene fossil mammal and plant localities of the Fort Union, Willwood, and Tatman formations, southern Bighorn Basin, Wyoming: U.S. Geological Survey Professional Paper 1540, p. 1–103.

Butler, R.F., Gingerich, P.D., and Lindsay, E.H., 1981, Magnetic polarity stratigraphy and biostratigraphy of Paleocene and lower Eocene continental deposits, Clarks Fork Basin, Wyoming: Journal of Geology, v. 89, p. 299–316.

Butler, R.F., Krause, D.W., and Gingerich, P.D., 1987, Magnetic polarity stratigraphy and biostratigraphy of middle-late Paleocene continental deposits of south-central Montana: Journal of Geology, v. 97, p. 647–657.

Cande, S.C., and Kent, D.V., 1992a, A new geomagnetic polarity time scale for the Late Cretaceous and Cenozoic: Journal of Geophysical Research, v. 97, p. 647–657.

Cande, S.C., and Kent, D.V., 1992b, Ultrahigh resolution marine magnetic anomaly profiles: A record of continuous paleointensity variations?: Journal of Geophysical Research, v. 97, p. 15,075–15,083.

Clyde, W.C., 1997, Stratigraphy and mammalian paleontology of the McCullough Peaks, northern Bighorn Basin, Wyoming: Implications for biochronology, basin development, and community reorganization across the Paleocene-Eocene boundary [Ph.D. thesis]: Ann Arbor, University of Michigan, 271 p.

Clyde, W.C., 2001, Mammalian biostratigraphy of the McCullough Peaks area in the northern Bighorn Basin, *in* Gingerich, P.D., ed., Paleocene-Eocene stratigraphy and biotic change in the Bighorn and Clarks Fork Basins, Wyoming: University of Michigan Papers on Paleontology, v. 33, p. 109–126.

Clyde, W.C., and Christensen, K.E., 2003, Testing the relationship between pedofacies and avulsion using Markov analysis: American Journal of Science, v. 303, p. 60–71, doi: 10.2475/ajs.303.1.60.

Clyde, W.C., and Gingerich, P.D., 1998, Mammalian community response to the latest Paleocene thermal maximum: An isotaphonomic study in the northern Bighorn Basin, Wyoming: Geology, v. 26, p. 1011–1014,doi: 10.1130/0091-7613(1998)026<1011:MCRTTL>2.3.CO;2.

Clyde, W.C., Stamatakos, J., and Gingerich, P.D., 1994, Chronology of the Wasatchian land-mammal age (early Eocene): Magnetostratigraphic results from the McCullough Peaks section, northern Bighorn Basin, Wyoming: Journal of Geology, v. 102, p. 367–377.

Clyde, W.C., Snell, K.E., Koch, P.L., Bowen, G.J., Chew, A.E., and Wing, S.E., 2006, Is ELMO in the Bighorn Basin? *in* Caballero F. et al, eds., Climate and Biota of the Early Paleogene 2006, Volume of Abstracts: Bilboa, Spain, p. 26.

Diehl, J.F., Beck, M.E., Jr., Beske-Diehl, S., Jacobson, D., and Hearn, B.C., Jr., 1983, Paleomagnetism of the Late Cretaceous–early Tertiary north-central Montana alkalic province: Journal of Geophysical Research, v. 88, p. 10,593–10,609.

Gingerich, P.D., 1983, Paleocene-Eocene faunal zones and a preliminary analysis of Laramide structural deformation in the Clark's Fork Basin, Wyoming: Wyoming Geological Association Thirty-Fourth Annual Field Conference Guidebook, p. 185–195.

Gingerich, P.D., 1991, Systematics and evolution of early Eocene Perissodactyla (Mammalia) in the Clarks Fork Basin, Wyoming: University of Michigan Museum of Paleontology Contributions, v. 28, p. 181–213.

Gradstein, F.M., Ogg, J.G., and Smith, A.G., 2004, A geologic time scale 2004: Cambridge, Cambridge University Press, 649 p.

Kirschvink, J.L., 1980, The least-squares line and plane and the analysis of paleomagnetic data: Royal Astronomical Society Geophysical Journal, v. 62, p. 743–746.

Koch, P.L., Zachos, J.C., and Dettman, D.L., 1995, Stable isotope stratigraphy and paleoclimatology of the Paleogene Bighorn Basin (Wyoming, USA): Palaeogeography, Palaeoclimatology, Palaeoecology, v. 115, p. 61–90, doi: 10.1016/0031-0182(94)00107-J.

Koch, P.L., Clyde, W.C., Hepple, R.P., Fogel, M.L., Wing, S.L., and Zachos, J.C., 2003, Carbon and oxygen isotope records from paleosols spanning the Paleocene-Eocene boundary, Bighorn Basin, Wyoming, *in* Wing, S.L., et al., eds., Causes and consequences of globally warm climates in the early Paleogene: Geological Society of America Special Paper 369, p. 49–64.

Kominz, M.A., and Pekar, S.F., 2001, Oligocene eustasy from two-dimensional sequence stratigraphic backstripping: Geological Society of America Bulletin, v. 113, p. 291–304, doi: 10.1130/0016-7606(2001)113<0291:OEFTDS>2.0.CO;2.

Kraus, M.J., 1997, Lower Eocene alluvial paleosols: Pedogenic development, stratigraphic relationships, and paleosol/landscape associations: Palaeogeography, Palaeoclimatology, Palaeoecology, v. 129, p. 387–406, doi: 10.1016/S0031-0182(96)00056-9.

Kraus, M.J., and Hasiotis, S.T., 2006, Significance of different modes of rhizolith preservation to interpreting paleoenvironmental and paleohydrologic settings: Examples from Paleogene paleosols, Bighorn Basin, Wyoming, U.S.A.: Journal of Sedimentary Research, v. 76, p. 633–646.

Lourens, L.J., Sluijs, A., Kroon, D., Zachos, J.C., Thomas, E., Rohl, U., Bowles, J., and Raffi, I., 2005, Astronomical pacing of late Palaeocene to early Eocene global warming events: Nature, v. 435, p. 1083–1087, doi: 10.1038/nature03814.

Lowrie, W., 1990, Identification of ferromagnetic minerals in rocks by coercivity and unblocking temperature properties: Geophysical Research Letters, v. 17, p. 159–162.

McMillan, M.E., Heller, P.L., and Wing, S.L., 2006, History and causes of post-Laramide relief in the Rocky Mountain orogenic plateau: Geological Society of America Bulletin, v. 118, p. 393–405, doi: 10.1130/B25712.1.

Roberts, A.P., and Winklhofer, M., 2004, Why are geomagnetic excursions not always recorded in sediments? Constraints from post-depositional remanent magnetization lock-in modeling: Earth and Planetary Science Letters, v. 227, p. 345–359, doi: 10.1016/j.epsl.2004.07.040.

Schankler, D.M., 1980, Faunal zonation of the Willwood Formation in the central Bighorn Basin, Wyoming, *in* Gingerich, P.D., ed., Early Cenozoic paleontology and stratigraphy of the Bighorn Basin, Wyoming: University of Michigan Papers on Paleontology, v. 24, p. 99–114.

Secord, R., Gingerich, P.D., Smith, M.E., Clyde, W.C., Wilf, P., and Singer, B.S., 2006, Geochronology and mammalian biostratigraphy of middle and upper Paleocene continental strata, Bighorn Basin, Wyoming: American Journal of Science, v. 306, p. 211–245.

Smith, T., Rose, K.D., and Gingerich, P.D., 2006, Rapid Asia–Europe–North America geographic dispersal of earliest Eocene primate *Teilhardina* during the Paleocene–Eocene Thermal Maximum: National Academy of Sciences Proceedings, v. 103, p. 11,223–11,227, doi: 10.1073/pnas.0511296103.

Steckler, M.S., and Watts, A.B., 1978, Subsidence of the Atlantic-type continental margin off New York: Earth and Planetary Science Letters, v. 41, p. 1–13, doi: 10.1016/0012-821X(78)90036-5.

Tauxe, L., Gee, J., Gallet, Y., Pick, T., and Bown, T., 1994, Magnetostratigraphy of the Willwood Formation, Bighorn Basin, Wyoming: New constraints on the location of the Paleocene/Eocene boundary: Earth and Planetary Science Letters, v. 125, p. 159–172, doi: 10.1016/0012-821X(94)90213-5.

Tauxe, L., and Watson, G., 1994, The fold test: An eigen analysis approach: Earth and Planetary Science Letters, v. 122, p. 331–341, doi: 10.1016/0012-821X(94)90006-X.

Watson, G.S., 1956, A test for randomness of directions: Royal Astronomical Society Geophysical Journal, Monthly Notices, v. 7, supplement, p. 160–161.

Watts, A.B., 2001, Isostasy and flexure of the lithosphere: Cambridge, Cambridge University Press, 458 p.

Wing, S.L., and Harrington, G.J., 2001, Floral response to rapid warming in the earliest Eocene and implications for concurrent faunal change: Paleobiology, v. 27, p. 539–563, doi: 10.1666/0094-8373(2001)027<0539:FRTRWI>2.0.CO;2.

Wing, S.L., Bown, T.M., and Obradovich, J.D., 1991, Early Eocene biotic and climatic change in interior western North America: Geology, v. 19, p. 1189–1192, doi: 10.1130/0091-7613(1991)019<1189:EEBACC>2.3.CO;2.

Wing, S.L., Alroy, J., and Hickey, L.J., 1995, Plant and mammal diversity in the Paleocene to early Eocene of the Bighorn Basin: Palaeogeography, Palaeoclimatology, Palaeoecology, v. 115, p. 117–155, doi: 10.1016/0031-0182(94)00109-L.

Wing, S.L., Bao, H., and Koch, P.L., 2000, An early Eocene cool period? Evidence for continental cooling during the warmest part of the Cenozoic, *in* Huber, B.T., et al., eds., Warm climates in Earth history: Cambridge, Cambridge University Press, p. 197–237.

Wu, W., and Wang, S.S.Y., 2006, Formulas for sediment porosity and settling velocity: Journal of Hydraulic Engineering, v. 132, p. 858–862, doi: 10.1061/(ASCE)0733-9429(2006)132:8(858).

Zijderveld, J.D.A., 1967, A.C. demagnetization of rocks: Analysis of results, *in* Collinson, D.W., et al., eds., Methods of palaeomagnetism: Amsterdam, Elsevier, p. 254–286.

Manuscript Received 13 September 2006
Revised Manuscript Received 5 January 2007
Manuscript Accepted 2 march 2007

Printed in the USA